

# Response of the North Atlantic subpolar gyre to persistent North Atlantic oscillation like forcing

Katja Lohmann · Helge Drange · Mats Bentsen

Received: 17 July 2007 / Accepted: 3 September 2008  
© Springer-Verlag 2008

**Abstract** The response of the North Atlantic subpolar gyre (SPG) to a persistent positive (or negative) phase of the North Atlantic oscillation (NAO) is investigated using an ocean general circulation model forced with idealized atmospheric reanalysis fields. The integrations are analyzed with reference to a base-line integration for which the model is forced with idealized fields representing a neutral state of the NAO. In the positive NAO case, the results suggest that the well-known cooling and strengthening of the SPG are, after about 10 years, replaced by a warming and subsequent weakening of the SPG. The latter changes are caused by the advection of warm water from the subtropical gyre (STG) region, driven by a spin-up of the Atlantic meridional overturning circulation (AMOC) and the effect of an anomalous wind stress curl in the north-eastern North Atlantic, which counteracts the local buoyancy forcing of the SPG. In the negative NAO case, however, the SPG response does not involve a sign reversal, but rather shows a gradual weakening throughout the integration. The asymmetric SPG-response to the sign of persistent NAO-like forcing and the different time scales involved demonstrate strong non-linearity in the North Atlantic Ocean circulation response to atmospheric forcing.

The latter finding indicates that analysis based on the arithmetic difference between the two NAO-states, e.g. NAO+ minus NAO−, may hide important aspects of the ocean response to atmospheric forcing.

**Keywords** North Atlantic subpolar gyre · Ocean's response to North Atlantic oscillation

## 1 Introduction

The North Atlantic subpolar gyre (SPG) has recently achieved considerable attention with regard to its strong and rapid variability, and far-reaching consequences for the (marine) climate in the northern North Atlantic. Häkkinen and Rhines (2004) report a strong weakening of the SPG circulation since the mid-1990s based on altimeter and hydrographic data. Hatun et al. (2005), by combining hydrographic and satellite observations and a hindcast simulation with an ocean general circulation model (OGCM), demonstrate that temperature and salinity throughout the northern rim of the SPG, and also of the inflow to the Nordic Seas, is tightly linked to the intensity of the SPG. It is therefore likely that the SPG influences the decadal-scale variability of the Atlantic meridional overturning circulation (AMOC) through precondition processes influencing the formation of intermediate and deep water masses both south and north of the Greenland-Scotland Ridge.

In a recent study using hindcast simulations with an OGCM, Böning et al. (2006) suggest that variations of the deep western boundary current off Labrador, as part of the SPG, reverberate into the strength of the subtropical AMOC and could therefore be used as part of an AMOC monitoring system. Furthermore, it is likely that the

---

K. Lohmann (✉) · H. Drange · M. Bentsen  
Nansen Environmental and Remote Sensing Center,  
Thormøhlensgate 47, 5006 Bergen, Norway  
e-mail: katja.lohmann@nersc.no

K. Lohmann · H. Drange · M. Bentsen  
Bjerknes Center for Climate Research, Bergen, Norway

H. Drange  
Geophysical Institute, University of Bergen, Bergen, Norway

H. Drange  
Nansen-Zhu International Research Center, Beijing, China

temporal and spatial abundance of both phytoplankton and zooplankton in the northeastern North Atlantic are, to a large degree, regulated by the structure and intensity of the SPG (H. Hatun, pers. comm 2008).

The variability of the circulation in the North Atlantic and, in particular, of the SPG has been linked, among other forcing mechanisms, to the North Atlantic oscillation (NAO), the dominant large-scale mode of atmospheric variability in the North Atlantic region (Hurrell 1995). Using hydrographic observations, Curry and McCartney (2001) constructed a time series of the baroclinic pressure difference between the centers of the subtropical gyre (STG) and the SPG. This transport index suggests a weakening of the North Atlantic gyre circulation during the low NAO period of the 1960s followed by a strengthening in the subsequent decades with high NAO. Changes in the STG region are primarily wind stress driven through vertical displacements of the main thermocline. Changes in the SPG region, on the other hand, are primarily thermally driven through surface buoyancy fluxes. Häkkinen and Rhines (2004), using altimeter and hydrographic data, report a decline of the SPG strength in the 1990s, which goes along with low NAO heat fluxes. Using hindcast simulations with an OGCM, Böning et al. (2006) suggest that the decline in the SPG is part of a decadal variability of the gyre transport driven by changes in both heat flux and wind stress associated with the NAO. Häkkinen (1999), also using hindcast simulations with an OGCM, suggests that the increase in the AMOC and the meridional heat transport in the 1980s and 1990s results from changes in the surface fluxes related to the NAO, which are integrated by the upper ocean. Using sensitivity experiments with a coupled atmosphere-ocean GCM, Delworth and Dixon (2000) show that a multidecadal positive trend in the Arctic Oscillation leads to an increase in the AMOC by about 15%. Eden and Willebrand (2001) as well as Brauch and Gerdes (2005), using OGCMs forced with idealized NAO-like surface fields based on the NCEP-NCAR reanalysis, suggest a delayed (interannual timescale) baroclinic response of the SPG and the AMOC

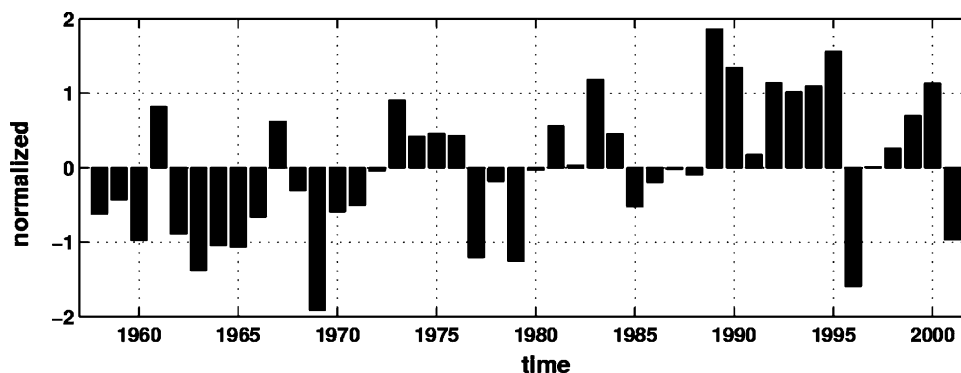
with an intensification (weakening) during a positive (negative) phase of the NAO. A comprehensive overview of the response of the North Atlantic and Arctic Ocean to an NAO-like forcing is provided by Visbeck et al. (2003) as well as by Furevik and Nilsen (2005), the latter for the Nordic Seas.

Here we use an OGCM forced with fields from the ERA40 reanalysis (Uppala et al., 2005) from the European Center for medium weather forecast (ECMWF) to further explore the response of the SPG to an idealized NAO-like forcing. In particular, we address the following two questions which so far have not received much attention in the literature:

- (i) *How does the SPG respond to a persistent, decadal time scale positive (negative) NAO forcing?* Time series of the NAO index show multi-annual periods of one NAO phase as well as a tendency for a positive NAO state in the recent decades (Hurrell et al. 2003; Fig. 1). It is therefore of relevance to examine the ocean response to a persistent positive (negative) NAO-like forcing not only on interannual but also on decadal time scales to fully explore the ocean's response to atmospheric forcing.
- (ii) *How linear is the response of an ocean forced with positive or negative phases of the NAO?* Understanding the non-linearity of the oceanic response as well as the underlying mechanisms is a topic of much interest. In addition, non-linearities may imply that the traditional way of viewing the ocean's response to positive and negative NAO forcing, i.e. through the arithmetic difference between the two states, might hide temporal and/or spatial characteristics that are not symmetrical.

The analysis presented in this paper is mainly devoted to the SPG response to a positive phase of the NAO, although the effect of negative NAO forcing is described as well. The reason for the focus on the positive NAO is that strong and apparently different responses on inter-annual and decadal time scales are found for this forcing.

**Fig. 1** NAO index based on the ERA40 reanalysis defined as difference of normalized winter (December–March) SLP between Lisbon, Portugal, and Reykjavik, Iceland



To account for the asymmetry in the atmospheric forcing patterns during phases of a positive and negative NAO (e.g. Cassou et al., 2004), we follow the approach of Brauch and Gerdes (2005) in which the idealized forcing fields are based on composites of individual positive and negative NAO years. In addition to previous studies, an idealized forcing representing a neutral state of the NAO is introduced to illuminate eventual non-linearities in the ocean's response to the different atmospheric forcing patterns representing a positive and negative NAO.

The paper is organized as follows: The OGCM and the conducted integrations are briefly described in Sect. 2. In Sect. 3 the SPG response to a positive NAO (with reference to a neutral NAO) is presented, and the results are discussed in Sect. 4.

## 2 Model description and experimental design

The OGCM used in this study is the Nansen Center version of the miami isopycnic coordinate ocean model (MICOM) forced with ERA40 reanalysis (Uppala et al. 2005) fields. In our version of MICOM, the core solvers are substituted with new numerical schemes, and it is estimated that about two-third of the code has been rewritten compared to the default MICOM-code as described in Bleck and Smith (1990) and Bleck et al. (1992). One major difference is that the Nansen Center version of MICOM conserves heat and salt by the introduction of incremental remapping (Dukowicz and Baumgardner 2000) as the transport method. The remapping method also ensures that layer thicknesses and tracers are treated in a fully consistent way. The Nansen Center version of MICOM has been used in several previous studies (e.g. Nilsen et al. 2003; Bentsen et al. 2004; Gao et al. 2004; Drange et al. 2005; Hatun et al. 2005).

The grid configuration used in this study is global with an almost regular horizontal grid spacing of approximately  $2.4^\circ$  latitude by  $2.4^\circ$  longitude. Near the equator, the meridional grid spacing is gradually decreased towards  $0.8^\circ$  at the equator. To circumvent grid singularities in the computational ocean domain, the North Pole of the grid is located over central Siberia (see Fig. 1b in Furevik et al. 2003). The horizontal grid spacing in the North Atlantic is about 150 km. Vertically, 35 isopycnic layers are used with potential densities ranging from  $\sigma_\theta = 21.22$  to  $\sigma_\theta = 28.70$ .

To maintain a stable and realistic AMOC, a Newtonian relaxation of sea surface salinity (SSS) is applied with a relaxation time scale of 30 days for a 50 m thick mixed layer, linearly decreasing with thicker mixed layers (see Bentsen et al. 1999). No relaxation was applied in waters where sea-ice is present in March in the Arctic and in September in the Antarctic to avoid relaxation towards

salinity outliers in the poorly sampled polar waters. In addition, the mismatch between model and climatology were limited to  $|\Delta\text{SSS}| < 0.5$  psu in the computation of the relaxation fluxes. This avoids extreme fluxes in, for instance, the vicinity of the western boundary currents which are not realistically separated from the coast with the current model resolution. Continental runoff is included by adding freshwater into the appropriate coastal grid cells (Furevik et al. 2003).

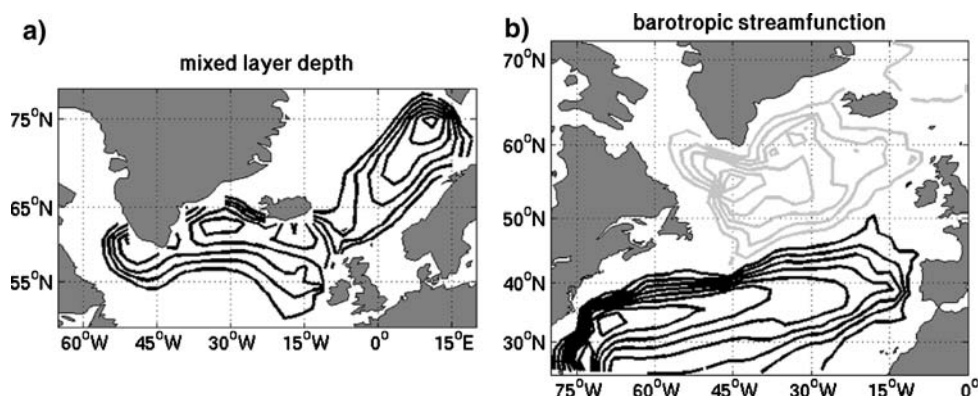
The ERA40 reanalysis data provide radiative fluxes and turbulent surface fluxes of momentum and heat, along with information of the ocean surface state (temperature and sea ice concentration). The forcing scheme and procedure proposed in Bentsen and Drange (2000) is used here. The scheme reproduces the reanalysis fluxes if the model has the same surface state as in the reanalysis. These states will generally differ and then the fluxes are modified. The turbulent fluxes are modified consistent with the bulk parameterization of Fairall et al. (1996) whereas the long-wave radiative fluxes are modified consistent with the Berliand and Berliand (1952) parameterization. Concerning the fresh water flux, the precipitation is provided by the ERA40 reanalysis directly and the evaporation is calculated based on the (modified) latent heat flux.

The model is spun up using six consecutive cycles of daily ERA40 reanalysis fields for the period from 1958 to 2001. For each cycle, the initial ocean state of the new integration is taken from the end state of the previous integration, yielding a total spin-up period of about 250 years. For the initial cycle, the hydrography is based on the January Levitus and Boyer (1994) and Levitus et al. (1994) climatological temperature and salinity fields, respectively, an ocean at rest, and a 2 m thick sea ice cover with extent according to climatology.

The convection sites in the model configuration used here are located southwest and southeast of Greenland as well as in the Nordic Seas (Fig. 2a). At all sites, convective mixing in March reaches below 800 m depth. The convection southeast of Greenland (in the Irminger Sea) might be overestimated in this model configuration. In a higher resolution version of the model (40 km in the North Atlantic) the convection in the Irminger Sea is reduced to about 500 m depth. Comparing the simulated exchange with the Nordic Seas to observations (Hansen et al., 2008), a too strong Atlantic inflow (about 13 Sv) is found in our model configuration. This overestimation seems to be related to the relatively coarse horizontal resolution, as the higher resolution version simulates an Atlantic inflow of 8 Sv which is close to the observed value. The sea ice distribution in our model configuration is in good agreement with observations.

As will be demonstrated shortly, the strength of the AMOC is important for the response of the SPG to a

**Fig. 2** (a) Mean mixed layer depth in March and (b) mean barotropic streamfunction for spin-up cycle six. Contour interval is (a) 100 m (starting from 400 m) and (b) 5 Sv (starting from  $\pm 5$  Sv). Black (grey) contour lines represent positive (negative) values



positive phase of the NAO. Figure 3 displays the maximum strength of the AMOC for the last four spin-up cycles. The simulated mean strength of the AMOC is about 17 Sverdrup ( $1 \text{ Sv} = 10^6 \text{ m}^3 \text{ s}^{-1}$ ). Considering the variability, the strength of the AMOC increases by about 3 Sv from the mid-1960s to the mid-1980s. The behavior of the AMOC is similar to hind-cast integrations using the same model forced with NCEP-NCAR reanalysis fields (Kalnay et al. 1996; not discussed here) for the period 1948–2004, and is in qualitative agreement with other modelling studies (e.g. Häkkinen 1999; Haak et al. 2003; Bentsen et al. 2004; de Coetlogon et al. 2006).

The strength of the SPG for the last four spin-up cycles together with the strength derived from altimeter data is presented in Fig. 4. Here we define the SPG strength by averaging the sea surface height (SSH) over the SPG region bounded by  $60^\circ\text{W}$ – $15^\circ\text{W}$  and  $50^\circ\text{N}$ – $65^\circ\text{N}$ . Note that negative (positive) SSH anomalies correspond to a strong (weak) SPG. The OGCM used in this study simulates the relatively strong SPG until the mid-1990s and the subsequent weakening of the SPG, a change that is confirmed by altimeter data (e.g. Häkkinen and Rhines 2004). The simulated weakening during the recent years is, however, stronger than the observed weakening. This is true also for the same model forced with the NCEP-NCAR reanalysis (not shown). The reason for this deficiency is not yet clear.

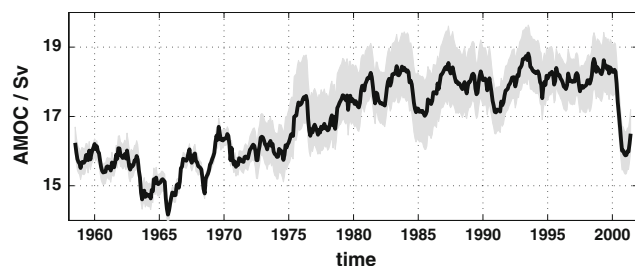


**Fig. 3** Monthly maximum strength ( $\text{Sv}$ ;  $1 \text{ Sv} = 10^6 \text{ m}^3 \text{ s}^{-1}$ ) of the AMOC between  $30$  and  $50^\circ\text{N}$  for spin-up cycles 3–6. A one-year running mean filter is applied. The black line shows the ensemble mean and the shading indicates the ensemble spreading

Horizontal grid spacing might play a role, since Hatun et al. (2005) using a nested and higher (20 km) resolution version of an OGCM similar to the one used in this study obtain a better agreement between the simulated and observed North Atlantic gyre circulation strength. Considering the strength of the SPG obtained from the barotropic streamfunction, a value of about 30 Sv is simulated in our model configuration (Fig. 2b). Note that the SPG index used in the analysis (Sect. 3) is defined as the SPG strength averaged over the subpolar North Atlantic. This area-averaged SPG strength is about 11 Sv in the spin-up simulations.

After the spin-up phase, the OGCM is forced for 40 years with idealized ERA40 reanalysis fields representing conditions during persistently positive ( $\text{NAO}^+$ ) and neutral ( $\text{NAO}^0$ ) states of the NAO. The idealized forcing fields are constructed in the following way: Forcing representing  $\text{NAO}^+$  conditions is defined as the monthly composite mean of the years 1983, 1989, 1990, 1992, 1994, 1995 and 2000, plus the daily variability (with respect to monthly means of the individual year) of the individual  $\text{NAO}^+$  years. The model response is then examined by cycling through these seven years. Forcing representing  $\text{NAO}^0$  conditions is defined analogously using the years 1972, 1978, 1980, 1982, 1987, 1988 and 1997, whereas negative NAO years ( $\text{NAO}^-$ ) consist of the years 1963, 1964, 1965, 1969, 1977, 1979 and 1996. A year is here defined from July to June (with the year number indicated by January) to avoid joining the individual years in boreal winter when the NAO forcing is most active (Hurrell et al. 2003). The monthly averaging of several years will smooth out unusual values or characteristics in one or several of the forcing components for an individual year, which are independent from the NAO.

The choice of the  $\text{NAO}^+$ ,  $\text{NAO}^-$  and  $\text{NAO}^0$  years is based on the NAO index defined as the winter (December–March) sea level pressure (SLP) difference between Lisbon and Reykjavik calculated from the ERA40 reanalysis (Fig. 1). The index based on the ERA40 reanalysis is in

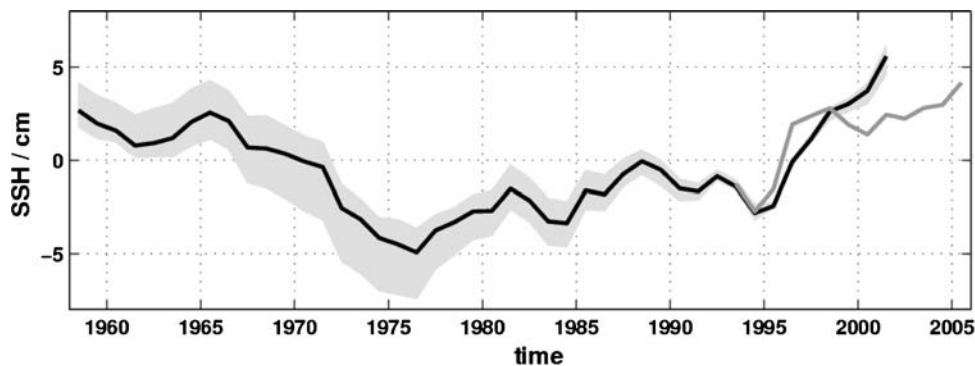
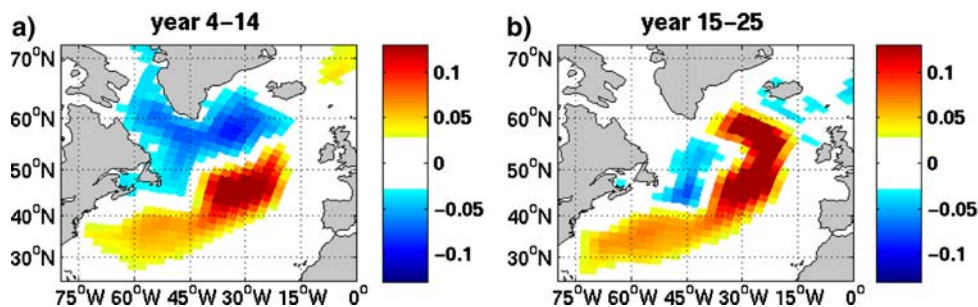


**Fig. 4** Annual SSH anomalies (cm; with respect to the 1993–1999 mean) averaged over the North Atlantic SPG region (60–15°W, 50–65°N) for spin-up cycles 3–6 (black line shows ensemble mean and shading indicates ensemble spreading). The grey line is the

corresponding SSH anomalies from the Ssalto/Duacs altimeter data (from [http://www.jason.oceanobs.com/html/donnees/duacs/welcome\\_uk.html](http://www.jason.oceanobs.com/html/donnees/duacs/welcome_uk.html)). Note that negative (positive) anomalies correspond to a stronger (weaker) SPG

**Fig. 5** Difference in the SSH (m) between the NAO<sup>+</sup> and NAO<sup>n</sup> integration. Initial conditions are from July 1961, and panel a (b) is averaged over integration years 4–14 (15–25)



good agreement with available station data (Hurrell et al. 2003). The NAO<sup>+</sup> years are chosen as the years for which the NAO index exceeds plus one standard deviation (seven years). The NAO<sup>n</sup> years are chosen as the 7 years for which the NAO index is closest to zero.

We have performed idealized NAO integrations using different initial conditions. The integrations given most emphasis in this study start from July 1961 (from the last spin-up cycle). In the 1960s, the strength of the simulated AMOC is weak (Fig. 3). However, the strength of the AMOC increases between the mid-1960s and mid-1980s. A second set of NAO<sup>+</sup> and NAO<sup>n</sup> integrations is therefore performed using July 1983 as initial conditions. In this way, the sensitivity experiments explore the ocean's response with respect to an ocean state characterized by weak and strong AMOC. In addition, we perform a NAO<sup>+</sup> integration starting from July 1995, i.e. after a period with a rather persistently positive NAO forcing (1989–1995, Fig. 1).

### 3 Response of the SPG to persistent positive NAO forcing

A key finding from the integrations driven by NAO-like forcing is the difference in the response of the North

Atlantic SPG to NAO<sup>+</sup> conditions lasting for inter-annual and decadal timescales. In Fig. 5, this difference is exemplified as the difference in the SSH between the NAO<sup>+</sup> and NAO<sup>n</sup> integrations starting in July 1961 (in the following we will always refer to the difference between the NAO<sup>+</sup> and the NAO<sup>n</sup> integration, even if this is not stated explicitly).

In Fig. 5a, the SSH difference is averaged over integration years 4–14. As discussed below, the lag between the SPG and the NAO-like buoyancy forcing is about two years. Therefore, the first 3 years of the idealized experiments are not taken into account here. Initially, both the SPG and the STG strengthen under NAO<sup>+</sup> conditions as described previously (e.g. Curry and McCartney 2001; Eden and Willebrand 2001). Note that for the cyclonic SPG, negative SSH anomalies correspond to a strengthening of the gyre.

During phases of a positive NAO, strong cold winds over the northern North Atlantic lead, through the large loss of heat from the ocean, to surface cooling in the SPG region. The time series of the mixed layer temperature averaged over the SPG shows an initial decrease of more than 0.5°C for the NAO<sup>+</sup> integration (Fig. 6, black dashed curve, until about year seven). The strongest temperature anomalies of about 1°C are found in the eastern SPG (Fig. 7a).

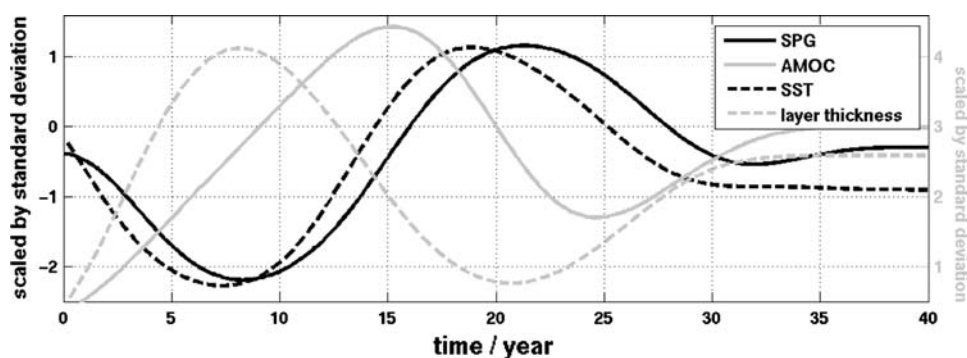
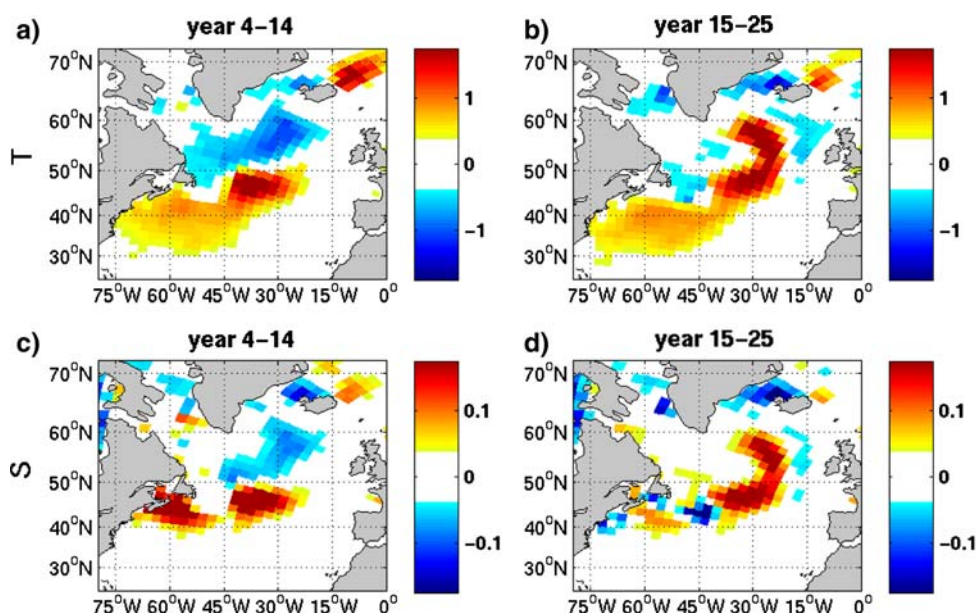


**Fig. 6** Difference between the  $\text{NAO}^+$  and  $\text{NAO}^-$  integration (initial conditions from July 1961) for the barotropic streamfunction (black line), the mixed layer temperature (black dashed line) and the thickness of the layers with potential density between  $\sigma_\theta = 27.65$  and  $\sigma_\theta = 27.72$  (grey dashed line, right y-axis), all averaged over the North Atlantic SPG region ( $53\text{--}65^\circ\text{N}$ ,  $60\text{--}15^\circ\text{W}$ ). The grey line (right y-axis) shows the maximum (between  $30$  and  $50^\circ\text{N}$  and throughout

the water column)) strength of the AMOC. A 10-year lowpass filter and scaling by the associated standard deviations have been applied to the time series. One standard deviation corresponds to  $1.8\text{ Sv}$  for the barotropic streamfunction,  $0.3^\circ\text{C}$  for the mixed layer temperature,  $154\text{ m}$  for the layer thickness, and  $0.8\text{ Sv}$  for the strength of the AMOC. Note that for the streamfunction negative (positive) values correspond to a strong (weak) SPG

**Fig. 7** Difference in the mixed layer temperature ( $^\circ\text{C}$ ; upper panels) and salinity (psu; lower panels) between the  $\text{NAO}^+$  and  $\text{NAO}^-$  integration. Initial conditions are from July 1961. Panels **a** and **c** (**b** and **d**) are averaged over integration years 4–14 (15–25)



Through cooling and subsequent formation of intermediate to deep water masses, the  $\text{NAO}^+$ -like buoyancy forcing leads to an initial increase in the thickness of the density layers with potential density between  $\sigma_\theta = 27.65$  and  $\sigma_\theta = 27.72$  (see Fig. 6, grey dashed curve, until about year seven). The latter density layers, approximately occupying the depth range around  $1500\text{ m}$ , are in the following called the intermediate layers. The maximum change in the thickness of the intermediate layers (up to  $1000\text{ m}$ ) is found in the eastern SPG (Fig. 9a). This should, at least partly, be due to the fact that the deepest mixing anomalies in the  $\text{NAO}^+$  integration are found in the Irminger Sea.

The thickening of the intermediate layers creates a doming structure of the isopycnals in the SPG, which leads

to an initial strengthening of the SPG (Fig. 6, black curve, until about year eight; note that negative values of the SPG index correspond to a stronger gyre). We here define the SPG index by averaging the barotropic streamfunction over the region  $53\text{--}65^\circ\text{N}$  and  $60\text{--}15^\circ\text{W}$ . The  $53^\circ\text{N}$  boundary is chosen as it approximately represents the boundary between the SPG and the STG in the  $\text{NAO}^+$  integration (Fig. 5a). The barotropic streamfunction is chosen because it is more representative for defining the strength of the SPG than the SSH. The response of the SPG lags behind the mixed layer temperature by about 2 years, as seen also from the corresponding cross correlation function (not shown). This time lag is within the range of what has been suggested by other modelling studies (e.g. Eden and Willebrand 2001; Dong and Sutton 2005; Bellucci and

Richards 2006). The increase in the SPG index under  $\text{NAO}^+$  conditions is about 4 Sv, or 30% of the mean SPG index in the  $\text{NAO}^n$  integration.

The formation of intermediate to deep water masses under  $\text{NAO}^+$  conditions also strengthens the AMOC, although on a longer time scale, as can be seen from the time series of the maximum strength of the AMOC (Fig. 6, grey curve, until about year 15). The strength of the AMOC lags behind the mixed layer temperature and the thickness of the intermediate layers by about 7 years, as seen also from the corresponding cross correlation function (not shown). The increase in the strength of the AMOC under  $\text{NAO}^+$  conditions is about 3.5 Sv, or 20% of the mean strength of the AMOC in the  $\text{NAO}^n$  integration. It is noteworthy that the strength of the AMOC in the  $\text{NAO}^+$  integration (without reference to  $\text{NAO}^n$ ) reaches a value (about 19 Sv) similar to that found in the spin-up from the mid-1990s when a positive NAO forcing has been dominating (Fig. 3). The response of the AMOC to the NAO-like forcing is consistent with previous modelling studies (e.g. Häkkinen 1999; Delworth and Dixon 2000; Eden and Willebrand 2001; Brauch and Gerdes 2005).

The spin-up of the AMOC, especially the North Atlantic current (NAC) component of the AMOC, leads to the advection of warm (Fig. 7b, 8d) and saline (Fig. 7d, 8f) water from the STG into the eastern part of the SPG region

(note that Fig. 8e, f display the haline contribution to the steric height, so anomalies in salinity have opposite sign to the fields in Fig. 7c, d).

Additionally, the wind stress curl in the northeastern North Atlantic will contribute to the extension of subtropical water into the SPG region. Under  $\text{NAO}^+$  conditions the negative wind stress curl over the STG extends further into the northeastern North Atlantic (Fig. 10). Figure 7 illustrates the replacement of the initially cold and fresh SPG mixed layer water by the warmer and more saline water from the south. The largest increase in mixed layer temperature (about  $3^\circ\text{C}$ ) and salinity (about 0.3 psu) is found in the eastern SPG, where the influences of the NAC and the wind stress curl are strongest. The influence of advection on the SST in the SPG region counteracting the local buoyancy fluxes related to the NAO has been described in previous studies. Eden and Jung (2001), using an OGCM driven by realistic forcing fields associated with the NAO, find, for certain periods, the development of interdecadal SST anomalies against the local damping influence from the NAO due to the lagged (10–20 years) response of the AMOC to interdecadal variability of the NAO. Also Visbeck et al. (1998), using an OGCM forced with NAO-like wind fields, find a warming of the SPG region under a positive NAO situation if the frequency of the NAO variability is low enough. In contrast

**Fig. 8** Difference in the steric height (m; surface to bottom) between the  $\text{NAO}^+$  and  $\text{NAO}^n$  integration: total (*upper panels*), thermal contribution (*middle panels*) and haline contribution (*lower panels*). Initial conditions are from July 1961. Panel a, c, e (b, d, f) are averaged over integration years 4–14 (15–25)

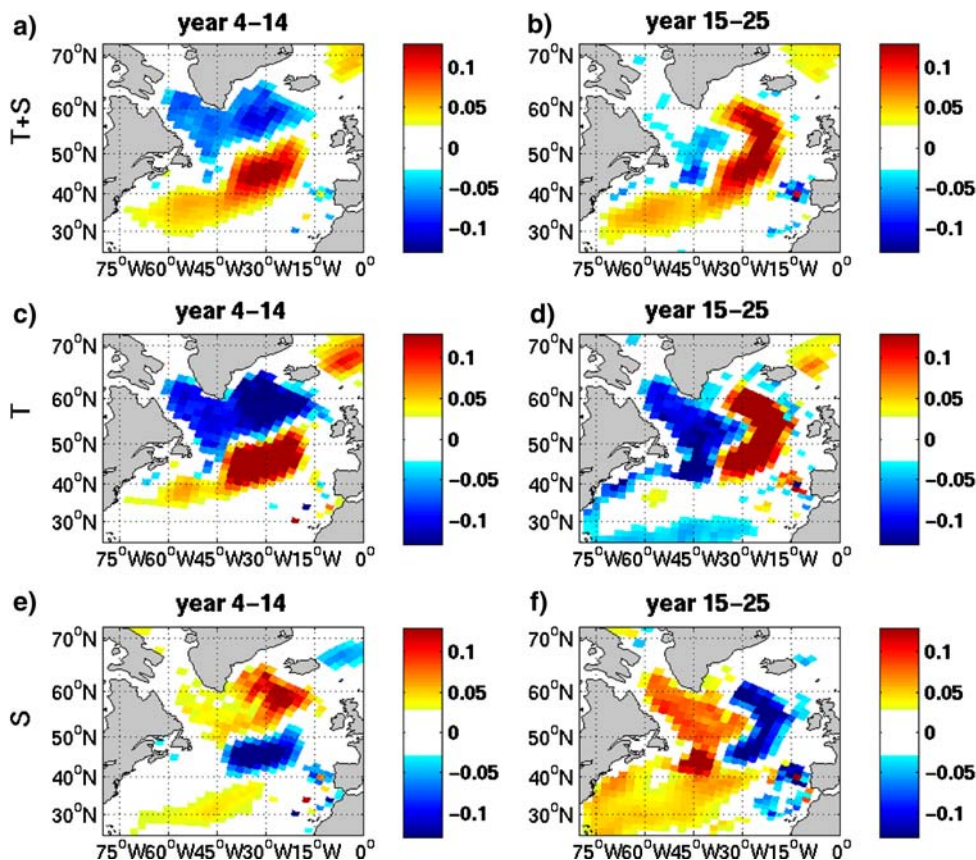
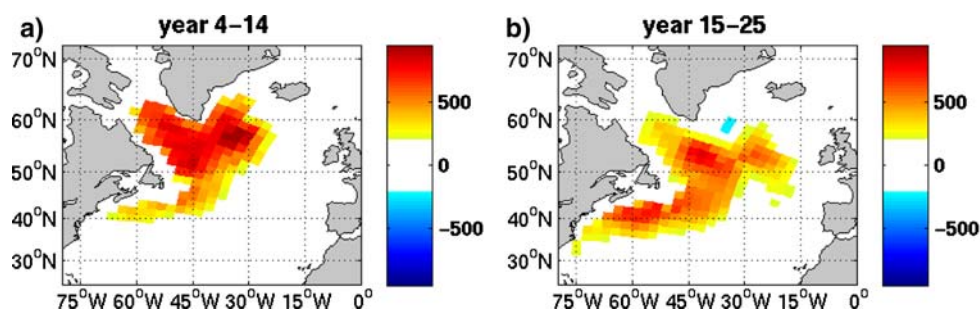


**Fig. 9** Difference in the thickness (m) of the layers with potential density between  $\sigma_\theta = 27.65$  and  $\sigma_\theta = 27.72$  between the NAO<sup>+</sup> and NAO<sup>n</sup> integration. Initial conditions are from July 1961. Panel (a) is averaged over integration years 4–14 (15–25)



to our study, however, this response seems to be based on the generation of temperature anomalies off the North American east coast by NAO related wind stress, which propagate along the NAC pathway (Krahmann et al. 2001).

The increased buoyancy of the upper ocean, governed by increased temperature, reduces the vertical winter-time mixing as well as the duration of this mixing. Consequently, the thickness of the intermediate layers will decrease (Fig. 9b). Maximum changes in the thickness of the intermediate layers in the eastern SPG are of the order of 1,000 m. Figure 9 also suggests a south- and eastward propagation of the intermediate layer anomalies.

The time series of the mixed layer temperature and intermediate layer thickness show that the warming in the SPG region and the following decrease in the intermediate layer thickness start after about eight years of NAO<sup>+</sup> forcing (Fig. 6, black dashed and grey dashed curve respectively). They lag behind the increase in the AMOC by 5–6 years as can also be seen from the corresponding cross correlation function (not shown). A similar lag between the AMOC and the temperature in the SPG region is also found in an analysis of the Hadley Centre climate model by Dong and Sutton (2005).

The decrease in the thickness of the intermediate layers leads to a decay of the domed structure of the isopycnals in the SPG, which in turn will decrease the strength of the gyre (Fig. 5b). Note that the wind forcing does not change between the realizations shown in Fig. 5a, b. The weakening of the SPG in our integration starts after about nine years of NAO<sup>+</sup> forcing, as seen from the SPG index

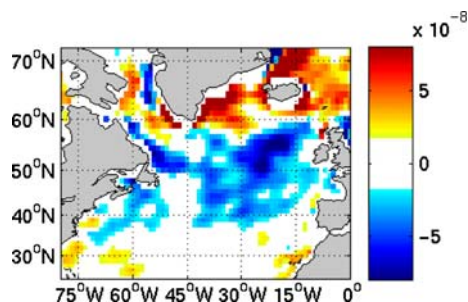


**Fig. 10** Difference between the average wind stress curl ( $\text{N m}^{-3}$ ) for the idealized NAO<sup>+</sup> and NAO<sup>n</sup> forcing, respectively

(Fig. 6, black curve), lagging behind the mixed layer temperature by about two years (as discussed above). The decrease in the SPG index is about 6 Sv, or 50% of the mean SPG index in the NAO<sup>n</sup> integration.

Considering the changes in the SSH (Fig. 5), the general pattern as well as the order of the changes are well represented by changes in the steric height (Fig. 8a, b). In the SPG region south of Iceland the changes in the steric height (surface to bottom) amount to about 20–30 cm. By dividing the steric height changes up into the thermal and haline contributions, it follows that the changes in the steric height are dominated by temperature (Fig. 8c, d), partially counteracted by salinity (Fig. 8e, f). The dominance of the temperature effect on the density in the SPG region is consistent with observed changes in the hydrography in the region (Hatun et al. 2005; Siegmund et al. 2007). The change in the steric height taking only the temperature contribution is about 50 cm in the eastern SPG region, corresponding to changes in the vertically integrated heat content of  $7 \text{ GJ m}^{-2}$ .

The time series in Fig. 6 show a damped oscillatory behavior suggesting that the system goes through an internal adjustment before reaching a new steady state (after about year 30). This adjustment is based on the fact that a thinning (thickening) of the intermediate layers leads to a weakening (strengthening) of the AMOC, which, through the reduced (enhanced) poleward advection of warm water, will in turn lead to a thickening (thinning) of the intermediate layers. Note that the atmospheric momentum forcing remains unchanged and the SST dependency on the buoyancy forcing is minimal throughout the integration. An internal adjustment of the AMOC to changes in the deep water formation is the basis for decadal variability in many studies using ocean only and coupled climate models (e.g. Delworth et al. 1993; Eden and Greatbach 2003; Bentsen et al. 2004; Dong and Sutton 2005). In contrast to this study, however, some of the papers suggest that the density anomalies in the sinking region are dominated by salinity anomalies. Figure 6 also suggests that the response of the SPG after about 30 years of NAO<sup>+</sup> forcing is much smaller than the initial response due to the internal adjustment of the ocean circulation.

To investigate if the response of the SPG to the NAO-like forcing depends on the ocean initial state, apart from the  $\text{NAO}^+$  and  $\text{NAO}^n$  integration starting from July 1961 (described so far), we analyze the SPG response in integrations starting from initial conditions in July 1983 and July 1995. Between the mid-1960s and the mid-1980s the strength of the AMOC increases by about 3 Sv (Fig. 3). Additionally, the mid-1990s represent an ocean state after a period of a rather persistently positive NAO forcing (1989–1995). To avoid starting a  $\text{NAO}^n$  integration from 1995, the  $\text{NAO}^+$  integration starting from the mid-1990s is considered with reference to the  $\text{NAO}^n$  integration starting from July 1983. Note that the strength of the AMOC as well as the SPG is similar in the early 1980s and mid-1990s (Figs. 3 and 4).

In the integrations starting from an initial condition representing a stronger AMOC, the initial strengthening of the SPG is reduced (Fig. 11b compared to Fig. 11a). The strengthening is further reduced if the initial conditions represent conditions after a period of several years with positive NAO forcing (Fig. 11c). The above mentioned reduction is about 30 and 60% for initial conditions in the early 1980s and mid-1990s, respectively. We also calculated SPG indices for the integrations with initial conditions in the early 1980s and mid-1990s (not shown) by averaging the barotropic streamfunction over the SPG region as shown in Fig. 6 (black curve) for the integration with initial conditions in the 1960s. The indices suggest that also for the integrations starting from initial conditions representing a stronger AMOC, the weakening of the SPG starts after about 10 years of  $\text{NAO}^+$  conditions. The amplitude of the oscillation seen in Fig. 6 (black curve) is,

however, reduced in the integrations with initial conditions representing a stronger AMOC.

#### 4 Discussion

In the previous section we have described the response of the North Atlantic SPG to a persistent (decadal scale)  $\text{NAO}^+$  forcing. Our results are based on integrations performed with a relatively coarse resolution version of the OGCM (horizontal grid spacing of about 150 km in the region of interest). Coarser resolution models tend to have a pathway of the subtropical water with a too northerly extension (heading towards Iceland), thereby favoring a warming and a subsequent weakening of the SPG. Furthermore, our coarse resolution model configuration tends to favour deep mixing in the Irminger Sea. To investigate the sensitivity of our results to the horizontal resolution, we perform 20 year long  $\text{NAO}^+$  and  $\text{NAO}^n$  integrations (initial conditions from July 1961) using the same model but with a grid configuration with focus in the North Atlantic Ocean and a horizontal resolution of about 40 km in the region of interest. The analysis shows a qualitatively similar response of the SPG between the two model versions, with an initial strengthening which is gradually replaced by a weakening under persistent  $\text{NAO}^+$  forcing. We therefore strongly believe that the obtained ocean response described in Sect. 3 is not critically dependent on the grid resolution.

In a previous study, Brauch and Gerdes (2005, hereafter BG05) analyze the response of the North Atlantic Ocean to a sudden drop in the NAO using a geopotential ( $z$ -level) coordinate OGCM. They perform integrations where a

**Fig. 11** Difference in the SSH (m) between the  $\text{NAO}^+$  and  $\text{NAO}^n$  integrations with initial conditions from July 1961 (a), July 1983 (b) and July 1995 (c), averaged over integration years 4–14. Note that panel a is the same as Fig. 4a, but with adjusted color scale

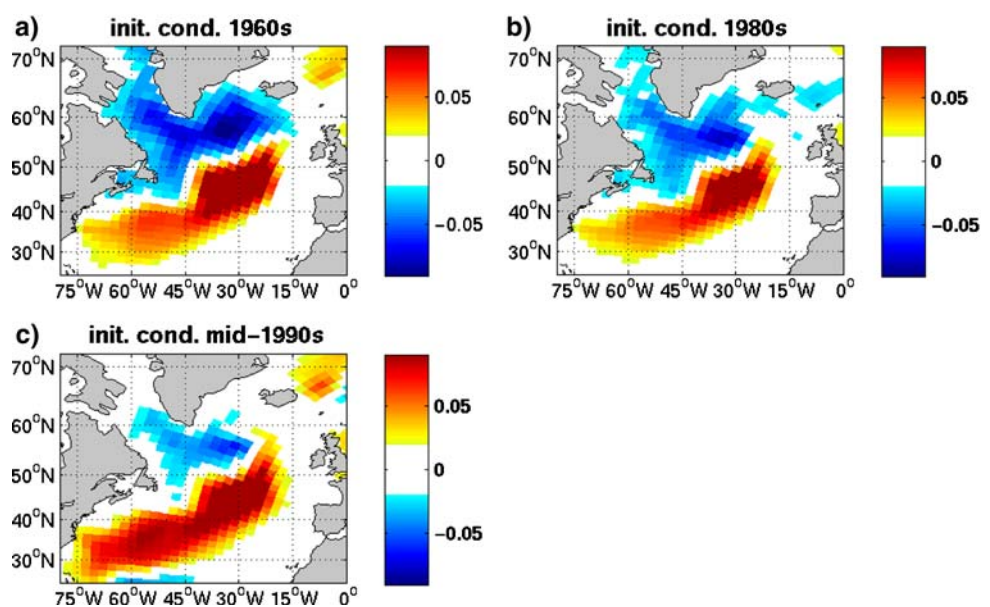
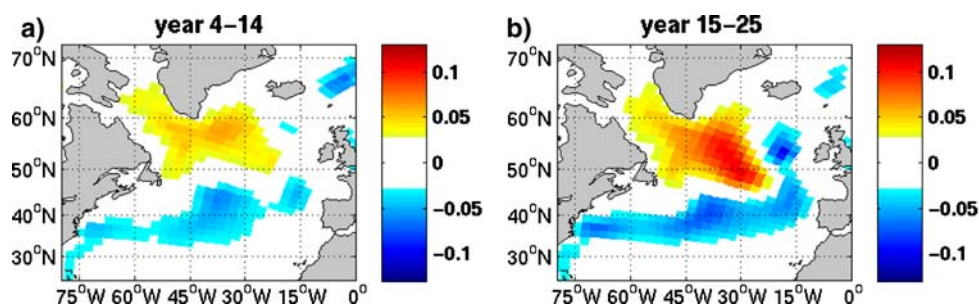


**Fig. 12** Same as Fig. 4, but for the difference between the  $\text{NAO}^-$  and  $\text{NAO}^n$  integration



200 year long spin-up with a  $\text{NAO}^+$ -type of forcing was followed by ten years with idealized  $\text{NAO}^-$  forcing (their SWITCH experiment) or continued for ten more years with the  $\text{NAO}^+$  forcing (their CONTROL experiment). Due to the spin-up with  $\text{NAO}^+$  forcing, the SPG in CONTROL in BG05 is closest to the SPG in our  $\text{NAO}^+$  integration after about integration year 15. Since the response time scale of the SPG to the  $\text{NAO}$ -like buoyancy forcing is a few years, our  $\text{NAO}^-$  integration (started from a spin-up with a realistic rather than a persistently positive  $\text{NAO}$  forcing) should be comparable to SWITCH in BG05 at integration year ten. The difference patterns in both BG05 and our study show a weakening (strengthening) of the SPG circulation under  $\text{NAO}^-$  ( $\text{NAO}^+$ ) conditions and an extension of the STG into the northeastern North Atlantic. The similarity with BG05 provides further confidence in our results as two different OGCMs (level versus layer) as well as two different reanalysis products (NCEP-NCAR versus ERA40) are used.

The patterns shown in Figs. 7b, d and 8d, f suggest a poleward advection of warm and saline water from the STG under persistent  $\text{NAO}^+$  conditions. It is noteworthy that in the  $\text{NAO}^+$  integration the mean southward volume transport (not ice) through the Denmark and Davis Strait is increased by about 10% compared to the mean transports in the  $\text{NAO}^n$  integration. This is true for both the coarse and the higher (40 km) resolution versions of our OGCM. The increased volume transports bring relatively cold and fresh water from the Arctic into the SPG region, which will, although to a limited extent, counteract the poleward advection of warm and saline subtropical water.

The ocean's response to persistent  $\text{NAO}^-$  forcing is very different from the situation with persistent  $\text{NAO}^+$  forcing discussed so far. Figure 12 displays the evolution of the SSH in the  $\text{NAO}^-$  integration (with reference to the  $\text{NAO}^n$  integration). Both an initial (panel a) and continued (panel b) increase of the subpolar SSH is found, implying a gradual, monotonic weakening of the SPG. The weakening is, however, approaching a minimum and the pattern shown in Fig. 12b remains nearly unchanged after integration year 25.

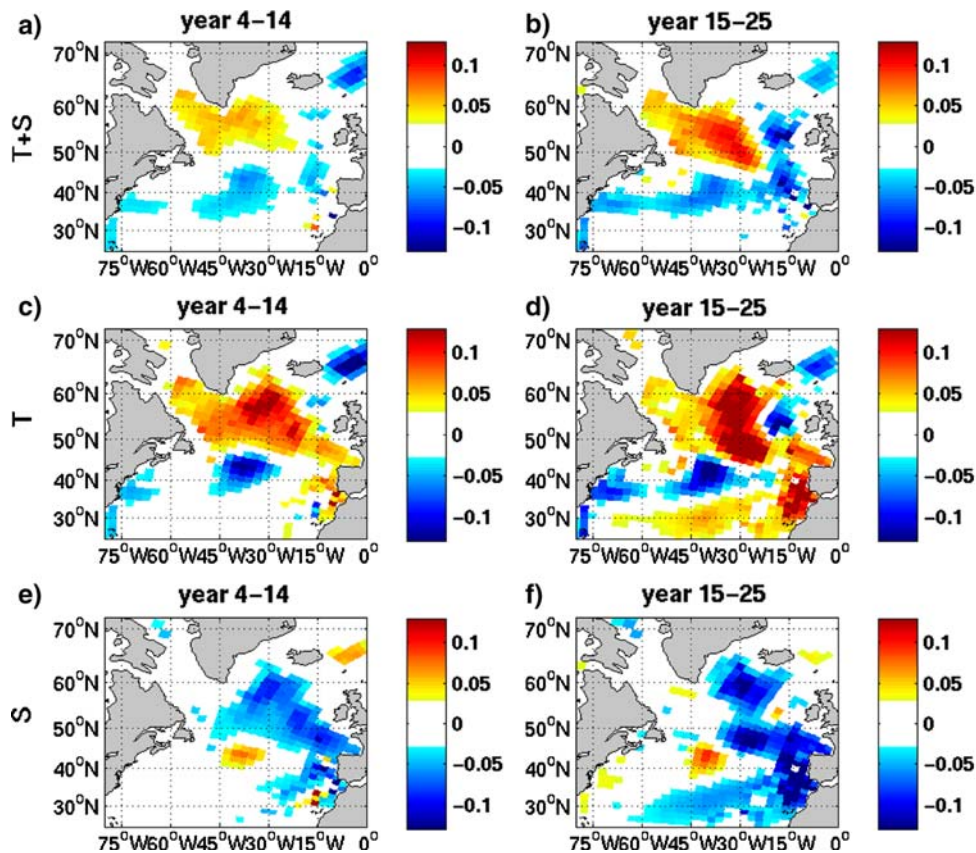
By comparing the spatial response of the North Atlantic gyre circulation between the  $\text{NAO}^+$  (Fig. 5a) and the  $\text{NAO}^-$  (Fig. 12a) integration, a pronounced tilt of the boundary between the SPG and the STG is found under  $\text{NAO}^+$  conditions, while the gyre boundary is more zonal under  $\text{NAO}^-$  conditions. This spatial non-linearity is consistent with the findings from Marshall et al. (2001) using a simplified mathematical model. Also the amplitude of the initial gyre response is different between the two integrations, being weaker under  $\text{NAO}^-$  than under  $\text{NAO}^+$  conditions. Comparing mixed layer temperature anomalies (not shown) suggests that the warming effect under  $\text{NAO}^-$  conditions is weaker than the cooling effect under  $\text{NAO}^+$ , which should contribute to the difference in the gyre response.

In Fig. 13 the evolution of the steric height and the corresponding thermal and haline contributions for persistent  $\text{NAO}^-$  forcing is shown. In sharp contrast to Fig. 8, no advective signals are seen in the evolution of the thermal and haline contributions. Although the AMOC decreases by about 2 Sv in the case of  $\text{NAO}^-$  forcing (due to reduced formation rates of intermediate and deep waters), no gradual cooling of the SPG region, which would counteract the local buoyancy forcing, is found (Fig. 13d). The absence of poleward advection of salt to the SPG region (oceanic response to the atmospheric forcing), together with no anomalous heat loss to the atmosphere under  $\text{NAO}^-$  conditions (atmospheric forcing itself), inhibit intermediate to deep mixing and thus the formation of intermediate to deep waters throughout the integration period, resulting in the monotonic weakening of the circulation.

As a motivation for this study we have posed the questions: (1) *how does the SPG respond to persistent positive (negative)  $\text{NAO}$  forcing?* and (2) *are there non-linearities in the ocean's response to  $\text{NAO}^+$  and  $\text{NAO}^-$  forcing?* The presented analysis can be summarized as follows:

Under persistent  $\text{NAO}^+$  forcing the well-known initial strengthening of the SPG is, after about 10 years, replaced by a weakening of the gyre. This change in the gyre is caused by the delayed but strong AMOC response to the

**Fig. 13** Same as Fig. 10, but for the difference between the  $NAO^-$  and  $NAO^0$  integration



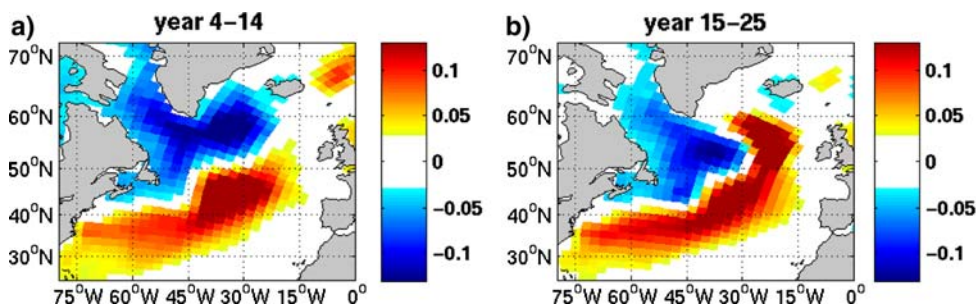
formation of intermediate and deep waters in the SPG region under  $NAO^+$  forcing. In particular, the spin-up of the AMOC is associated with the poleward advection of warm surface water from the STG counteracting the local buoyancy forcing in the SPG region. In contrast, a steady weakening of the SPG is found throughout the integration with  $NAO^-$  forcing. In this case, there is no ocean advective feedback.

Therefore, the ocean response to persistent  $NAO^+$  forcing is modulated by the poleward advection of warm water, counteracting the cooling effect of the atmosphere. Importantly, the associated poleward advection (and thus densification) of salt is secondary to temperature, see Fig. 8 and discussions above. In contrast, the ocean response to persistent  $NAO^-$  forcing is monotonic due to the absence

of poleward advection of salt, implying continued low formation rates of intermediate and deep waters.

In Fig. 14 the SSH pattern based on the  $NAO^+$  minus the  $NAO^-$  integration is shown. The pattern suggest an extension of the STG into the northeastern North Atlantic, but *not* a weakening of the SPG under persistent  $NAO^+$  conditions. The temporal and spatial non-linearity of the ocean's response to  $NAO^+$  and  $NAO^-$  forcing strongly indicates that more insight may be gained in analyzing the responses relative to an intermediate state like  $NAO^0$ , for instance along the lines of the analysis in this study. Further analysis of the non-linearities of the North Atlantic and Arctic Ocean's response is beyond the scope of this paper, but remains an important issue to improve our understanding of the inter-annual to decadal scale variability of

**Fig. 14** Same as Fig. 4, but for the difference between the  $NAO^+$  and  $NAO^-$  integration



the North Atlantic climate, its predictability, and possible ecosystem changes derived thereof.

**Acknowledgments** This work has been supported by the European Union through the DYNAMITE project (GOCE-003903) and by the Research Council of Norway through the NorClim and NOTUR projects. The ECMWF ERA-40 data used in this study have been obtained from the ECMWF Data Server (<http://www.ecmwf.int/products/data/archive/>). The altimeter products were produced by Ssalto/Duacs and distributed by Aviso ([http://www.jason.oceanobs.com/html/donnees/duacs/welcome\\_uk.html](http://www.jason.oceanobs.com/html/donnees/duacs/welcome_uk.html)), with support from CNES. We thank three anonymous reviewers for their valuable comments on an earlier version of the manuscript. Fruitful discussions with other scientists from the Nansen and Bjerknes Centers, especially Anne-Britt Sandø and Jan Even Øie Nilsen, as well as with the project partners, are greatly acknowledged. This is contribution A173 from the Bjerknes Centre for Climate Research.

## References

- Bellucci A, Richards K (2006) Effects of NAO variability on the North Atlantic Ocean circulation. *Geophys Res Lett* 33:L02612. doi:10.1029/2005GL024890
- Bentsen M, Evensen G, Drange H, Jenkins A (1999) Coordinate transformation on a sphere using conformal mapping. *Mon Weather Rev* 127:2733–2740. doi:10.1175/1520-0493(1999)127<2733:CTOASU>2.0.CO;2
- Bentsen M, Drange H (2000) Parameterizing surface fluxes in ocean models using the NCEP/NCAR reanalysis data. RegClim general technical report no. 4, Norwegian Institute for Air Research, 149–158
- Bentsen M, Drange H, Furevik T, Zhou T (2004) Simulated variability of the Atlantic meridional overturning circulation. *Clim Dyn* 22:701–720. doi:10.1007/s00382-004-0397-x
- Berliand M, Berliand T (1952) Determining the net long-wave radiation of the earth with consideration of the effect of cloudiness. *Isv Akad Nauk SSSR Ser Geofis* 1:11–16
- Bleck R, Smith L (1990) A wind-driven isopycnic coordinate model of the north and equatorial Atlantic Ocean. 1. Model development and supporting experiments. *J Geophys Res* 95:3273–3285. doi:10.1029/JC095iC03p03273
- Bleck R, Rooth C, Hu D, Smith L (1992) Salinity-driven thermocline transients in a wind- and thermohaline-forced isopycnic coordinate model of the North Atlantic. *J Phys Oceanogr* 22:1486–1505. doi:10.1175/1520-0485(1992)022<1486:SDTTIA>2.0.CO;2
- Böning C, Scheinert M, Dengg J, Biastoch A, Funk A (2006) Decadal variability of subpolar gyre transport and its reverberation in the North Atlantic overturning. *Geophys Res Lett* 33:L21S01. doi:10.1029/2006GL026906
- Brauch J, Gerdes R (2005) Response of the northern North Atlantic and Arctic oceans to a sudden change of the North Atlantic Oscillation. *J Geophys Res* 110. doi:10.1029/2004JC002436
- Cassou C, Terray L, Hurrell J, Deser C (2004) North Atlantic winter climate regimes: spatial asymmetry, stationarity with time and oceanic forcing. *J Clim* 17:1055–1068. doi:10.1175/1520-0442(2004)017<1055:NAWCRS>2.0.CO;2
- Curry R, McCartney M (2001) Ocean gyre circulation changes associated with the North Atlantic oscillation. *J Phys Oceanogr* 31:3374–3400. doi:10.1175/1520-0485(2001)031<3374:OGCCAW>2.0.CO;2
- de Coetlogon G, Frankignoul C, Bentsen M, Delon C, Haak H, Masina S et al (2006) Gulf Stream variability in five oceanic general circulation models. *J Phys Oceanogr* 36:2119–2135. doi:10.1175/JPO2963.1
- Delworth T, Manabe S, Stouffer R (1993) Interdecadal variations of the thermohaline circulation in a coupled ocean-atmosphere model. *J Clim* 6:1993–2011. doi:10.1175/1520-0442(1993)006<1993:IVOTTC>2.0.CO;2
- Delworth T, Dixon K (2000) Implications of the recent trend in the Arctic/North Atlantic oscillation for the North Atlantic thermohaline circulation. *J Clim* 13:3721–3727. doi:10.1175/1520-0442(2000)013<3721:IOTRTI>2.0.CO;2
- Dong B, Sutton R (2005) Mechanism of interdecadal thermohaline circulation variability in a coupled ocean-atmosphere GCM. *J Clim* 18:1117–1135. doi:10.1175/JCLI3328.1
- Drange H, Gerdes R, Gao Y, Karcher M, Kauker F, Bentsen M (2005) Ocean general circulation modelling of the Nordic Seas. In: Drange H, Dokken T, Furevik T, Gerdes R, Berger W (eds) *The Nordic Seas: an integrated perspective*, AGU monograph 158. American Geophysical Union, Washington, DC
- Dukowicz J, Baumgardner J (2000) Incremental remapping as a transport/advection algorithm. *J Comput Phys* 160:318–335. doi:10.1006/jcph.2000.6465
- Eden C, Jung T (2001) North Atlantic interdecadal variability: oceanic response to the North Atlantic oscillation (1865–1997). *J Clim* 14:676–691. doi:10.1175/1520-0442(2001)014<0676:NAIVOR>2.0.CO;2
- Eden C, Willebrand J (2001) Mechanism of inter-annual to decadal variability of the North Atlantic circulation. *J Clim* 14:2266–2280. doi:10.1175/1520-0442(2001)014<2266:MOITDV>2.0.CO;2
- Eden C, Greatbach R (2003) A damped decadal oscillation in the North Atlantic climate system. *J Clim* 16:4043–4060. doi:10.1175/1520-0442(2003)016<4043:ADDOIT>2.0.CO;2
- Fairall C, Bradley E, Rogers D, Edson J, Young G (1996) Bulk parameterization of air-sea fluxes for tropical ocean–global atmosphere coupled ocean atmosphere response experiment. *J Geophys Res* 101:3747–3764. doi:10.1029/95JC03205
- Furevik T, Bentsen M, Drange H, Kindem I, Kvamstø N, Sorteberg A (2003) Description and evaluation of the Bergen climate model: ARPEGE coupled with MICOM. *Clim Dyn* 21:27–51. doi:10.1007/s00382-003-0317-5
- Furevik T, Nilsen E (2005) Large-scale atmospheric circulation variability and its impacts on the Nordic Seas ocean climate—a review. In: Drange H, Dokken T, Furevik T, Gerdes R, Berger W (eds) *The Nordic Seas: an integrated perspective*, AGU monograph 158. American Geophysical Union, Washington, DC
- Gao Y, Drange H, Bentsen M, Johannessen O (2004) Simulating transport of non-Chernobyl <sup>137</sup>Cs and <sup>90</sup>Sr in the North Atlantic–Arctic region. *J Environ Radioact* 71:1–16. doi:10.1016/S0265-931X(03)00108-5
- Haak H, Jungclauss J, Mikolajewicz U, Latif M (2003) Formation and propagation of great salinity anomalies. *Geophys Res Lett* 30. doi:10.1029/2003GL017065
- Häkkinen S (1999) Variability of the simulated meridional heat transport in the North Atlantic for the period 1951–1993. *J Geophys Res* 104:10991–11008. doi:10.1029/1999JC900034
- Häkkinen S, Rhines P (2004) Decline of subpolar North Atlantic circulation during the 1990s. *Science* 304:555–559. doi:10.1126/science.1094917
- Hansen B, Østerhus S, Turrell B, Jónsson S, Valdimarsson H, Hátún H, et al (2008) The inflow of Atlantic water, heat, and salt to the Nordic Seas across the Greenland-Scotland Ridge. In: Dickson D, Meincke J, Rhines P (eds.), *Arctic–subarctic ocean fluxes: defining the role of the Northern Seas in climate*, Springer-Verlag, due for release
- Hatun H, Sandø A-B, Drange H, Hansen B, Valdimarsson H (2005) Influence of the Atlantic subpolar gyre on the thermohaline circulation. *Science* 309:1841–1844. doi:10.1126/science.1114777

- Hurrell J (1995) Decadal trends in the North Atlantic oscillation: regional temperatures and precipitation. *Science* 269:676–679. doi:[10.1126/science.269.5224.676](https://doi.org/10.1126/science.269.5224.676)
- Hurrell J, Kushnir Y, Ottersen G, Visbeck M (2003) An overview of the North Atlantic oscillation. In: Hurrell J, Kushnir Y, Ottersen G, Visbeck M (eds) *The North Atlantic oscillation*, AGU Monograph 134. American Geophysical Union, Washington, DC
- Kalnay E et al (1996) The NCEP/NCAR 40-year reanalysis project. *Bull Am Meteorol Soc* 77:437–471. doi:[10.1175/1520-0477\(1996\)077<0437:TNYRP>2.0.CO;2](https://doi.org/10.1175/1520-0477(1996)077<0437:TNYRP>2.0.CO;2)
- Krahmann G, Visbeck M, Reverdin G (2001) Formation and propagation of temperature anomalies along the North Atlantic current. *J Phys Oceanogr* 31:1287–1303. doi:[10.1175/1520-0485\(2001\)031<1287:FAPOTA>2.0.CO;2](https://doi.org/10.1175/1520-0485(2001)031<1287:FAPOTA>2.0.CO;2)
- Levitus S, Boyer T (1994) *World Ocean atlas 1994, vol 4: temperature*. NOAA Atlas NESDIS 4, US Department of Commerce, Washington, DC, pp 117
- Levitus S, Burgett R, Boyer T (1994) *World Ocean Atlas 1994, vol 3: salinity*. NOAA Atlas NESDIS 3. US Department of Commerce, Washington, DC, pp 99
- Marshall J, Johnson H, Godman J (2001) A study of the interaction of the North Atlantic oscillation with ocean circulation. *J Clim* 14:1399–1421. doi:[10.1175/1520-0442\(2001\)014<1399:ASOTIO>2.0.CO;2](https://doi.org/10.1175/1520-0442(2001)014<1399:ASOTIO>2.0.CO;2)
- Nilsen J, Gao Y, Drange H, Furevik T, Bentsen M (2003) Simulated North Atlantic–Nordic Seas water mass exchanges in an isopycnic coordinate OGCM. *Geophys Res Lett* 30:1536–1539. doi:[10.1029/2002GL016597](https://doi.org/10.1029/2002GL016597)
- Siegismund F, Johannessen J, Drange H, Mork K, Korabely A (2007) Steric height variability in the Nordic Seas. *J Geophys Res* 112:C12010. doi:[10.1029/2007JC004221](https://doi.org/10.1029/2007JC004221)
- Uppala S et al (2005) The ERA-40 re-analysis. *QJR Meteorol Soc* 131:2961–3012. doi:[10.1256/qj.04.176](https://doi.org/10.1256/qj.04.176)
- Visbeck M, Chassignet E, Curry R, Delworth T, Dickson B, Krahmann G (2003) The ocean’s response to North Atlantic oscillation variability. In: Hurrell J, Kushnir Y, Ottersen G, Visbeck M (eds) *The North Atlantic oscillation*, AGU Monograph 134. American Geophysical Union, Washington, DC
- Visbeck M, Cullen H, Krahmann G, Naik N (1998) An ocean model’s response to North Atlantic oscillation-like wind forcing. *Geophys Res Lett* 25:4521–4524. doi:[10.1029/1998GL900162](https://doi.org/10.1029/1998GL900162)